Phase portraits of a family of Kolmogorov systems with infinitely many singular points at infinty

Érika Diz-Pita[a], Jaume Llibre[b], M. Victoria Otero-Espinar[a]

[a] *Departamento de Estatística, Análise Matemática e Optimización, Universidade de Santiago de Compostela, 15782 Santiago de Compostela, Spain*
[b] *Departament de Matemàtiques, Universitat Autònoma de Barcelona, 08193 Bellaterra, Barcelona, Spain*

Abstract

We give the topological classification of the global phase portraits in the Poincaré disc of the Kolmogorov systems

$$\dot{x} = x\left(a_0 + c_1 x + c_2 z^2 + c_3 z\right),$$
$$\dot{z} = z\left(c_0 + c_1 x + c_2 z^2 + c_3 z\right),$$

which depend on five parameters and have infinitely many singular points at the infinity. We prove that these systems have 22 topologically distincs phase portraits.

Keywords: Kolmogorov system, Phase portrait, Poincaré disc

1. Introduction and statement of the main results

Kolmogorov systems are polynomial differential systems of the form $\dot{x_i} = x_i P_i(x_1, \ldots, x_n)$ for $i = 1, ..., n$, where P_i are polynomials. These include, for instance, Lotka-Volterra or May-Leonard systems. Kolmogorov systems can be used for modelling problems from different sciences as the evolution of competing species [4, 9, 26, 27, 32], plasma physics [20], hydrodynamics [8], chemical reactions [18], the study of black holes [7], and economic [16, 17, 34] or social problems, as the evolution of the number of internet users [15].

Recently, some works on the global dynamics of these systems have been carried out. For example, for the May-Leonard systems, which have the form

$$\dot{x} = x(1 - x - ay - bz),$$
$$\dot{y} = y(1 - bx - y - az),$$
$$\dot{z} = z(1 - ax - by - z),$$

their global dynamics on the Poincaré sphere when $a + b = 2$ or $a = b$ were studied in [5], and the case with $a + b = -1$ were studied in [6].

The global dynamics of some particular Lotka-Volterra systems on dimension three has also been described on the Poincaré sphere as in [1], where the authors give the global phase portraits of a system that appears in the study of black holes, or in [24] where the description of the global dynamics of a system previously proposed and studied in [21, 25, 33] is finally completed.

Also the global study of some families depending on a small number of parameters has been done, as in [23] where the authors study a family depending on two parameters, or in [22] where the family depends on three parameters but with some restrictions as all of them must be positive.

Email addresses: erikadiz.pita@usc.es (Érika Diz-Pita), jllibre@mat.uab.cat (Jaume Llibre), mvictoria.otero@usc.es (M. Victoria Otero-Espinar)

With the aim of studying the global dynamics of the general 3-dimensional Lotka-Volterra systems depending on 12 parameters,

$$\begin{aligned}\dot{x} &= x(a_0 + a_1x + a_2y + a_3z),\\ \dot{y} &= y(b_0 + b_1x + b_2y + b_3z),\\ \dot{z} &= z(c_0 + c_1x + c_2y + c_3z),\end{aligned} \tag{1.1}$$

in [11] and [12] the global dynamics of two families of Kolmogorov systems is studied. Those families are obtained from (1.1) assuming the existence of a rational first integral of degree two of the form $x^iy^jz^k$, by applying the Darboux theory of integrability. For the obtained families, the condition that they have a Darboux invariant of the form $x^\ell y^m e^{st}$ is required. Here we will focus on the family

$$\dot{x} = x\left(a_0 - \mu(c_1x + c_2z^2 + c_3z)\right), \quad \dot{z} = z\left(c_0 + c_1x + c_2z^2 + c_3z\right), \tag{1.2}$$

that depends on five parameters. This family is studied in [11] where the topological classification of the global phase portraits in the Poincaré disc is given for all the values of the parameters with $\mu \neq -1$.

The particular case with $\mu = -1$, in which all the singular points at infinty are singular points was not studied, so here we carry out the study of this case, i.e. we study the systems

$$\dot{x} = x\left(a_0 + c_1x + c_2z^2 + c_3z\right), \quad \dot{z} = z\left(c_0 + c_1x + c_2z^2 + c_3z\right), \tag{1.3}$$

under conditions

$$H = \left\{c_2 \neq 0, a_0 \geq 0, c_1 \geq 0, c_3 \geq 0, a_0 \neq c_0, a_0^2 + c_1^2 \neq 0\right\}.$$

In Section 4 of [11] a set of conditions is given and it is proved that Kolmogorov systems (1.2) can be reduced to satisfy such conditions either using symmetries, or eliminating known phase portraits, or eliminating phase portraits with infinitely many finite singular points. For instance, it is not necessary to study the cases in which these systems can be reduced to Lotka-Volterra systems in dimension two, as the global qualitative dynamics of those systems has been completely studied in [31]. Asumming $\mu = -1$ those conditions become the conditions H given above. Also from the mentioned results, if $a_0 = 0$ we can consider $c_0 > 0$, as for $c_0 < 0$ the results can be obtained by symmetry.

We give the topological classification of all global phase portraits of systems (1.3) on the Poincaré disc, and our main result is the following.

Theorem 1.1. *Kolmogorov systems* (1.3) *have* 22 *topologically distinct phase portraits in the Poincaré disc, given in Figure 1.*

In Section 2 we summarize the basic results and techniques that we need for proving Theorem 1.1. In Section 3 we give the classification of the local phase portraits of the finite singular points, in Section 4 we study the local phase portraits at the infinite singular points, and finally in Section 5 we prove Theorem 1.1.

2. Preliminaries

2.1. Poincaré compactification

Our objective is to study the dynamics of system (1.3) in $\mathbb{R}^2$ adding the infinity and The Poincaré compactification allow us to study the orbits of a polynomial differential system near the infinity (see Chapter 5 of [14]).

Consider a polynomial vector field $X = (P(x, y), Q(x, y))$ defined in $\mathbb{R}^2$ such that $d = \max\{\deg P, \deg Q\}$. We call the sphere $\mathbb{S}^2 = \left\{y \in \mathbb{R}^3 : y_1^2 + y_2^2 + y_3^2 = 1\right\}$ the *Poincaré sphere*. We will assume that our vector field is defined in the tangent plane to the Poincaré sphere at the point $(0, 0, 1)$.

We can define a vector field $\overline{X}$ on $\mathbb{S}^2\backslash\mathbb{S}^1$ by means of the differentials Df^+ and Df^- of the central projections $f^+ : \mathbb{R}^2 \to \mathbb{S}^2$ and $f^- : \mathbb{R}^2 \to \mathbb{S}^2$. The obtained vector field is defined at all points in $\mathbb{S}^1$ except at those over the equator $\mathbb{S}^1$, which correspond with the points at infinity of $\mathbb{R}^2$, but we can extend it analytically

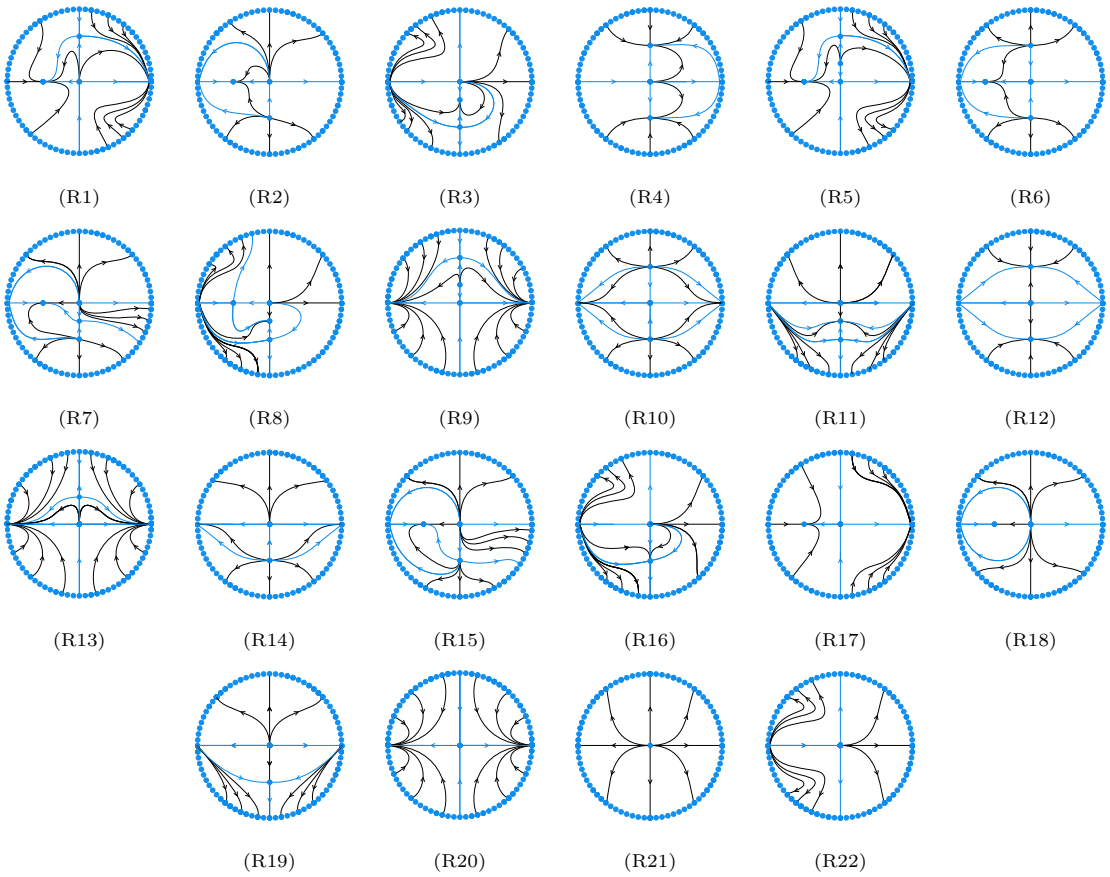

Figure 1: The topologically distincts phase portraits of systems (1.3) in the Poincaré disc.

to a vector field $\rho(X)$ defined on the closed Poincaré sphere multiplying by y_3^d. We say that $\rho(X)$ is the *Poincaré compactification* of the vector field X on $\mathbb{R}^2$.

To obtain the expressions of the vector field $\rho(X)$ we use the local charts (U_i, ϕ_i) and (V_i, ψ_i), where $U_i = \{y \in \mathbb{S}^2 : y_i > 0\}$, $V_i = \{y \in \mathbb{S}^2 : y_i < 0\}$, $\phi_i : U_i \longrightarrow \mathbb{R}^2$ and $\psi_i : V_i \longrightarrow \mathbb{R}^2$ for $i = 1, 2, 3$, with $\phi_i(y) = -\psi_i(y) = (y_m/y_i, y_n/y_i)$ for $m < n$ and $m, n \neq i$.

The expression of $\rho(X)$ in the local chart (U_1, ϕ_1) is

$$\dot{u} = v^d \left[-u\, P\left(\frac{1}{v}, \frac{u}{v}\right) + Q\left(\frac{1}{v}, \frac{u}{v}\right) \right], \ \dot{v} = -v^{d+1}\, P\left(\frac{1}{v}, \frac{u}{v}\right), \tag{2.1}$$

and in the local chart (U_2, ϕ_2) is

$$\dot{u} = v^d \left[P\left(\frac{1}{v}, \frac{u}{v}\right) - uQ\left(\frac{1}{v}, \frac{u}{v}\right) \right], \ \dot{v} = -v^{d+1}\, P\left(\frac{1}{v}, \frac{u}{v}\right). \tag{2.2}$$

We will not need the expression of $\rho(X)$ in the local chart (U_3, ϕ_3) and neither we need the explicit expressions of $\rho(X)$ in the local charts (V_i, ψ_i), with $i = 1, 2, 3$, as they can be obtained multiplying by $(-1)^{d-1}$ the expressions in (U_i, ϕ_i), so the behaviour will be the same as in those charts when d is even (the orientation should be reversed if d were odd).

The singular points of $\rho(X)$ which are over the equator are called the *infinite singular points* of X and if $p \in \mathbb{S}^1$ is an infinite singular point, then $-p$ is also an infinite singular point with the same stability if d is odd and opposite stability if d is even.

We will classify the global phase portraits of the Kolmogorov systems (1.3) in the Poincaré disc, which is the orthogonal projection of the closed northern hemisphere of $\mathbb{S}^2$ onto the plane $y_3 = 0$. This is enough to

get the complete classification because the orbits of $\rho(X)$ on $\mathbb{S}^2$ are symmetric with respect to the origin of $\mathbb{R}^3$.

2.2. Topological equivalence and separatrix skeleton

There are some important elements in a phase portrait that help us to carry out their topological classification. Special attention should be paid to the *separatrices*, namely, the orbits at the infinity, the finite singular points, the orbits on the boundary of a hyperbolic sector at a singular point and the limit cycles. Each of the connected components resulting from removing all separatrices from $\mathbb{D}^2$ are called *canonical regions*. By the *separatrix skeleton* of $\pi(\rho(X))$ we mean the union of all the separatrices together with an orbit of each canonical region.

In order to perform the topological classification, we recall the concept of topological equivalence. We say that two compactified polynomial differential systems in the Poincaré disc are *topologically equivalent* if there exists a homeomorphism that sends orbits to orbits preserving or reversing the orientation of all orbits.

Similarly, we say that two separatrix skeletons Σ_1 and Σ_2 are *topologically equivalent* if there is a homeomorphism $h : \mathbb{D}^2 \to \mathbb{D}^2$ such that $h(\Sigma_1) = \Sigma_2$.

To determine the topological classification of a polynomial differential system in the Poincaré disc it is enough to study the separatrix skeleton, as stated in the following result of Markus [28], Neumann [29] and Peixoto [30].

Theorem 2.1. *The phase portraits in the Poincaré disc of two compactified polynomial vector fields $\pi(\rho(X))$ and $\pi(\rho(Y))$ with finitely many separatrices are topologically equivalent if and only if their separatrix skeletons are topologically equivalent.*

This result applies to vector fields with finitely many separatrices, so we could not apply it to systems 1.3 in the closed Poincaré disc as they have infinitely many singular points at the inifinity, and so infinitely many separatrices, but we can apply it in the open Poincaré disc.

2.3. Desingularization of singular points

The first step to obtain the global phase portraits of our systems is to determine the local phase portraits at the singular points. For hyperbolic and semi-hyperbolic singular points we will use Theorem 2.15 and Theorem 2.19 in [14].

Whereas to study the singular points for which the Jacobian matrix is identically zero, called linearly zero points, we will need to go through a desingularization process, particularly we will use the blow up technique [2, 3].

Roughly speaking the blow up technique consist in explode the singular point to a line, and then study the new singular points that appear on that line. The process must be repeated if some of the new singular points are also linearly zero, but this is not a problem as it is proved by Dumortier in [13] that this iterative process is finite.

Let P and Q be coprime polynomials, P_m and Q_m homogeneous polynomials of degree $m \in \mathbb{N}$ and consider the differential system

$$\begin{aligned} \dot{x} &= P(x,y) = P_m(x,y) + o(m), \\ \dot{y} &= Q(x,y) = Q_m(x,y) + o(m), \end{aligned} \tag{2.3}$$

where $o(m)$ represents terms of order higher than m. The origin of this system is a singular point as $m > 0$, and we say that it is *nondicritical* if the *characteristic polynomial* $\mathcal{F}(x,y) := xQ_m(x,y) - yP_m(x,y)$ is not identically zero. We will only deal with nondicritical singular points on our study.

If we consider a new variable z, we say that the mapping $(x,y) \to (x,z) = (x, y/x)$ is a *homogeneous directional blow up in the vertical direction*. This map transforms the origin of (2.3) into the line $x = 0$ and we call this line the exceptional *exceptional divisor*. After this blow up system (2.3) becomes

$$\dot{x} = P(x,xz), \quad \dot{z} = \frac{Q(x,xz) - zP(x,xz)}{x}. \tag{2.4}$$

This system is always well-defined because we are assuming that the origin is a singular point.

Similarly, we say that the mapping $(x, y) \to (z, y) = (x/y, y)$ is a *homogeneous directional blow up in the horizontal direction.* In this case the exceptional divisor is the line $y = 0$ and the expression of the system is

$$\dot{z} = \frac{P(yz, y) - zQ(yz, y)}{y}, \quad \dot{x} = P(yz, y). \tag{2.5}$$

After the blow up in the vertical or horizontal direction, we cancel an appearing common factor x^{m-1}. The mapping swaps the second and the third quadrants in the vertical directional blow up and the third and the fourth quadrants in the horizontal blow up.The relationship between the behaviour at the origin of system (2.3) and the behaviour at the new singular points of system (2.4) is provided by Propositions 2.1 and 2.2 in [2], so we must study the singular points of system (2.4) on the exceptional divisor and then apply these results and undo the blow ups to determine the behaviour of the orbits around the origin of system (2.3). We recall that if some of these singular points on the exceptional divisor is linearly zero we have to repeat the process.

2.4. Normally hyperbolic submanifolds

Here we summarize a result that allows us to study systems which have a submanifold consisting of singular points, for more details see [10, 19]. If we have a smooth flow φ_t on a manifold M and C is a submanifold of M consisting entirely of singular points, we say that C is *normally hyperbolic* if the tangent bundle to M over C splits into three subbundles TC, E^s and E^u invariant under the flow and satisfying that $d\varphi_t$ contracts E^s exponentially, $d\varphi_t$ expands E^u exponentially and TC is the tangent bundle of C. For these submanifolds the following result holds:

Theorem 2.2. *Let C be a normally hyperbolic submanifold consisting of singular points for a flow φ_t. Then there exist smooth stable and unstable manifolds tangent along C to $E^s \oplus TC$ and $E^u \oplus TC$ respectively. Furthermore, both C and the stable and unstable manifolds are permanent under small perturbations of the flow.*

3. Local study of the finite singular points

From Section 5 in [11], if we consider the condition $\mu = -1$, we get that the singular points of systems (1.3) are

- $P_0 = (0, 0)$,
- $P_1 = \left(0, \dfrac{R_c - c_3}{2c_2}\right)$ and $P_2 = \left(0, -\dfrac{R_c + c_3}{2c_2}\right)$ if $c_3^2 > 4c_0c_2$;
- $P_3 = \left(0, -\dfrac{c_3}{2c_2}\right)$ if $c_3^2 = 4c_0c_2$;
- $P_4 = \left(-\dfrac{a_0}{c_1}, 0\right)$ if $c_1 \neq 0$.

From Table 1 in [11], we get six cases depending on the coexistence of finite singular points, given in Table 1.

Case	Conditions	Finite singular points
1	$c_3^2 > 4c_0c_2$, $c_1 \neq 0$.	P_0, P_1, P_2, P_4.
2	$c_3^2 > 4c_0c_2$, $c_1 = 0$, $a_0 \neq 0$.	P_0, P_1, P_2.
3	$c_3^2 = 4c_0c_2$, $c_1 \neq 0$.	P_0, P_3, P_4.
4	$c_3^2 = 4c_0c_2$, $c_1 = 0$, $a_0 \neq 0$.	P_0, P_3.
5	$c_3^2 < 4c_0c_2$, $c_1 \neq 0$.	P_0, P_4.
6	$c_3^2 < 4c_0c_2$, $c_1 = 0$, $a_0 \neq 0$.	P_0.

Table 1: The different cases for the finite singular points.

From Lemma 5.1 and Tables 2 to 7 in [11], asumming the condition $\mu = -1$, we get the following classification for the local phase portraits of the finite singular points, with 34 subcases.

Case 1: $\boldsymbol{c_3^2 > 4c_0c_2}$, $\boldsymbol{c_1 \neq 0}$.

Sub.	**Conditions**	**Classification**
1.1	$a_0 > 0$, $c_0 = 0$, $c_2 < 0$.	$P_0 \equiv P_1$ saddle-node, P_2 saddle, P_4 stable node.
1.2	$a_0 > 0$, $c_0 = 0$, $c_2 > 0$.	$P_0 \equiv P_1$ saddle-node, P_2 unstable node, P_4 stable node.
1.3	$a_0 = 0$, $c_0 > 0$, $R_c - c_3 < 0$, $c_2 > 0$.	$P_0 \equiv P_4$ saddle-node, P_1 stable node, P_2 saddle.
1.4	$a_0 = 0$, $c_0 > 0$, $c_2 < 0$, $R_c - c_3 > 0$.	$P_0 \equiv P_4$ saddle-node, P_1 stable node, P_2 stable node.
1.5	$a_0 > 0$, $c_0 < 0$, $c_2 < 0$, $a_0 - c_0 > 0$, $(R_c - c_3) < 0$.	P_0 saddle, P_1 unstable node, P_2 saddle, P_4 stable node.
1.6	$a_0 > 0$, $c_0 < 0$, $a_0 - c_0 > 0$, $c_2 > 0$, $R_c - c_3 > 0$.	P_0 saddle, P_1 unstable node, P_2 unstable node, P_4 stable node.
1.7	$a_0 > 0$, $c_0 > 0$, $a_0 - c_0 > 0$, $c_2 < 0$, $R_c - c_3 > 0$.	P_0 unstable node, P_1 saddle, P_2 saddle, P_4 stable node.
1.8	$a_0 > 0$, $c_0 > 0$, $R_c - c_3 < 0$, $a_0 - c_0 > 0$, $c_2 > 0$.	P_0 unstable node, P_1 saddle, P_2 unstable node, P_4 stable node.
1.9	$a_0 > 0$, $c_0 > 0$, $a_0 - c_0 < 0$, $R_c - c_3 < 0$, $c_2 > 0$.	P_0 unstable node, P_1 stable node, P_2 saddle, P_4 saddle.
1.10	$a_0 > 0$, $c_0 > 0$, $a_0 - c_0 < 0$, $c_2 < 0$, $R_c - c_3 > 0$.	P_0 unstable node, P_1 stable node, P_2 stable node, P_4 saddle.

Table 2: Classification in case 1 of Table 1 according with the local phase portraits of finite singular points.

Case 2: $\boldsymbol{c_3^2 > 4c_0c_2}$, $\boldsymbol{c_1 = 0}$, $\boldsymbol{a_0 > 0}$.

Sub.	**Conditions**	**Classification**
2.1	$c_0 < 0$, $a_0 - c_0 > 0$, $R_c - c_3 < 0$, $c_2 < 0$.	P_0 saddle, P_1 unstable node, P_2 saddle.
2.2	$c_0 < 0$, $a_0 - c_0 > 0$, $c_2 > 0$, $R_c - c_3 > 0$.	P_0 saddle, P_1 unstable node, P_2 unstable node.
2.3	$c_0 > 0$, $c_2(a_0 - c_0) < 0$, $R_c - c_3 > 0$.	P_0 unstable node, P_1 saddle, P_2 saddle.
2.4	$c_0 > 0$, $R_c - c_3 < 0$, $a_0 - c_0 > 0$, $c_2 > 0$.	P_0 unstable node, P_1 saddle, P_2 unstable node.
2.5	$c_0 > 0$, $a_0 - c_0 < 0$, $R_c - c_3 < 0$, $c_2 > 0$.	P_0 unstable node, P_1 stable node, P_2 saddle.
2.6	$c_0 > 0$, $a_0 - c_0 < 0$, $c_2 < 0$, $R_c - c_3 > 0$.	P_0 unstable node, P_1 stable node, P_2 stable node.
2.7	$c_0 = 0$, $a_0 > 0$, $c_2 < 0$.	$P_0 \equiv P_1$ saddle-node, P_2 saddle.
2.8	$c_0 = 0$, $a_0 > 0$, $c_2 > 0$.	$P_0 \equiv P_1$ saddle-node, P_2 unstable node.

Table 3: Classification in case 2 of Table 1 according with the local phase portraits of finite singular points.

Case 3: $\boldsymbol{c_3^2 = 4c_0c_2}$, $\boldsymbol{c_1 \neq 0}$.

Sub.	**Conditions**	**Classification**
3.1	$a_0 > 0$, $c_0 < 0$, $a_0 - c_0 > 0$.	P_0 saddle, P_3 saddle-node, P_4 stable node.
3.2	$a_0 > 0$, $c_0 > 0$, $a_0 - c_0 < 0$.	P_0 unstable node, P_3 saddle-node , P_4 saddle.
3.3	$a_0 > 0$, $c_0 > 0$, $a_0 - c_0 > 0$.	P_0 unstable node, P_3 saddle-node , P_4 stable node.
3.4	$a_0 = 0$, $c_0 > 0$.	$P_0 \equiv P_4$ saddle-node, P_3 saddle-node.
3.5	$c_0 = 0$, $a_0 > 0$, $c_2 < 0$.	$P_0 \equiv P_3$ topological saddle, P_4 stable node.
3.6	$c_0 = 0$, $a_0 > 0$, $c_2 > 0$.	$P_0 \equiv P_3$ topological unstable node, P_4 stable node.

Table 4: Classification in case 3 of Table 1 according with the local phase portraits of finite singular points.

Case 4: $c_3^2 = 4c_0c_2$, $c_1 = 0$, $a_0 > 0$.

Sub.	Conditions	Classification
4.1	$c_0 < 0$.	P_0 saddle, P_3 saddle-node.
4.2	$c_0 > 0$.	P_0 unstable node, P_3 saddle-node.
4.3	$c_0 = 0$, $c_2 < 0$.	$P_0 \equiv P_3$ topological saddle.
4.4	$c_0 = 0$, $c_2 > 0$.	$P_0 \equiv P_3$ topological unstable node.

Table 5: Classification in case 4 of Table 1 according with the local phase portraits of finite singular points.

Case 5: $c_3^2 < 4c_0c_2$, $c_1 \neq 0$.

Sub.	Conditions	Classification
5.1	$a_0 = 0$.	$P_0 \equiv P_4$ saddle-node.
5.2	$a_0 > 0$, $c_0 < 0$, $a_0 - c_0 > 0$.	P_0 saddle, P_4 stable node.
5.3	$a_0 > 0$, $c_0 > 0$, $a_0 - c_0 < 0$.	P_0 unstable node, P_4 saddle.
5.4	$a_0 > 0$, $c_0 > 0$, $a_0 - c_0 > 0$.	P_0 unstable node, P_4 stable node.

Table 6: Classification in case 5 of Table 1 according with the local phase portraits of finite singular points.

Case 6: $c_3^2 < 4c_0c_2$, $c_1 = 0$, $a_0 > 0$.

Sub.	Conditions	Classification
6.1	$c_0 < 0$.	P_0 saddle.
6.2	$c_0 > 0$.	P_0 unstable node.

Table 7: Classification in case 6 of Table 1 according with the local phase portraits of finite singular points.

4. Local study at the infinite singular points

In order to study the behaviour of the trajectories of systems (1.3) near infinity we consider the Poincaré compactification. We assume the hypothesis H. According to equations (2.1) and (2.2), we get the compactification in the local charts U_1 and U_2 respectively. To study all the infinite singular points, it is enough to study the singular points over $v = 0$ in the chart U_1 and the origin of the chart U_2.

We start with the study of the origin of the chart U_2, which is simpler. The systems in this chart have the expression

$$\dot{u} = (a_0 - c_0)uv^2, \quad \dot{v} = -c_1uv^2 - c_0v^3 - c_3v^2 - c_2v. \tag{4.1}$$

Over the line $v = 0$ we get $\dot{u}\,|_{v=0} = \dot{v}\,|_{v=0} = 0$, then all points at infinity are singular points, including the origin which is the only we must study in this chart. At the origin of this chart, one of the eigenvalues of the Jacobian matrix is zero and the other is $-c_2$. Applying Theorem 2.2 given in Subsection 2.4, we can conclude that if $c_2 > 0$ there is exactly one orbit outside the infinity that goes to the origin of U_2 and if $c_2 < 0$ there is exactly one orbit from outside the infinity that leaves the origin of U_2.

Now we address the study of the infinite singular points in the local chart U_1, where the expression of the systems is

$$\dot{u} = (c_0 - a_0)uv^2, \quad \dot{v} = -c_2u^2v - c_3uv^2 - a_0v^3 - c_1v^2. \tag{4.2}$$

Taking $v = 0$ we get again that all points at infinity in this chart are singular points. At the origin, the eigenvalues of the Jacobian matrix are both zero. At a point $(u_0, 0)$ with $u_0 \neq 0$ the eigenvalues are one zero and the other $-c_2u_0^2$ so, if $c_2 > 0$, then the nonzero eigenvalue is negative and exactly one orbit outside the infinity arrives at each infinite singular point on the chart U_1 distinct from the origin. If $c_2 < 0$ the nonzero eigenvalue is positive so from each inifinite singular point on the chart U_1 distinct from the origin leaves exactly one orbit from outside the infinity.

From the previous reasonings we can state the following result.

Lemma 4.1. *For any infinite singular point of systems* (1.3) *distinct from the origin of the chart* U_1 *the following statements hold:*

- *If* $c_2 > 0$ *exactly one orbit outside the infinity arrives to the singular point.*
- *If* $c_2 < 0$ *exactly one orbit from outside the infinity leaves the singular point.*

Now we must study insightfully the origin of the chart U_1, which we will name O_1. For this singular point we will prove the following result.

Lemma 4.2. *The origin of the chart* U_1 *is an infinite singular point of systems* (1.3) *and it has* 12 *distinct local phase portraits described in Figure 2.*

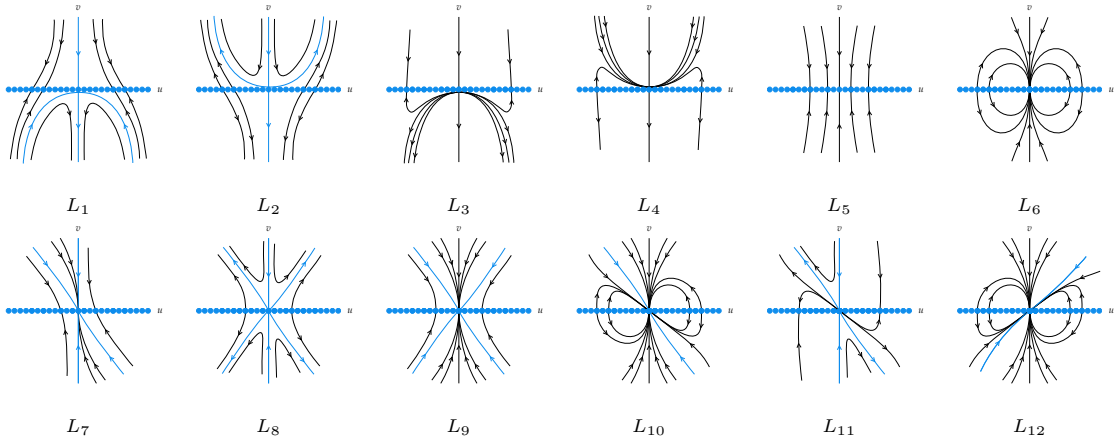

Figure 2: Local phase portraits at the infinite singular point O_1.

To prove Lemma 4.2, at first, we must eliminate a common factor v from systems (4.2) obtaining:

$$\dot{u} = (c_0 - a_0)uv, \quad \dot{v} = -c_2u^2 - c_3uv - a_0v^2 - c_1v. \tag{4.3}$$

Now we must study the origin of this system, which we name $\tilde{O}_1$, and which is now the only singular point over $v = 0$. The eigenvalues of the Jacobian matrix at $\tilde{O}_1$ are zero and $-c_1$, so if $c_1 \neq 0$ the singular point of system (4.3) is semi-hyperbolic and we can study it applying Theorem 2.19 of [14]. If $c_1 = 0$ we must study this singular point with the blow up technique.

4.1. Case with $\tilde{O}_1$ *semi-hyperbolic*

In order to apply the theorem for semi-hyperbolic singular points in [14], we must change the sign of the flow, as the result requires the nonzero eigenvalue to be positive. We obtain systems

$$\dot{u} = (a_0 - c_0)uv, \quad \dot{v} = c_2u^2 + c_3uv + a_0v^2 + c_1v, \tag{4.4}$$

and applying the mentioned result we get that the origin of these systems is a saddle point if $c_2(a_0 - c_0) > 0$ and a topological unstable node if $c_2(a_0 - c_0) < 0$. Then, reversing the orientations, the singular point $\tilde{O}_1$ is a saddle if $c_2(a_0 - c_0) > 0$ and a topological stable node if $c_2(a_0 - c_0) < 0$. Before obtaining the corresponding phase portraits for O_1, we will distinguish four cases according to the sign of c_2 and $a_0 - c_0$.

(a) If $c_2 > 0$ and $a_0 - c_0 > 0$ then $\tilde{O}_1$ is a saddle as in Figure 3(a). If we multiply by v to go back to systems (4.2), then all the points at the u-axis become singular points and the orientation of the orbits in the third and fourth quadrants is reversed. Thus, for O_1 we obtain the local phase portrait in Figure 3(b), which is L_1 of Figure 2.

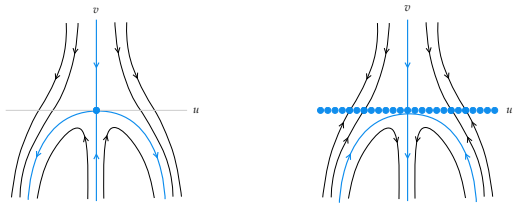

(a) Origin of systems (4.3) (b) Origin of systems (4.2)

Figure 3: Local phase portraits of $\tilde{O}_1$ and O_1 with $c_2 > 0$ and $a_0 - c_0 > 0$.

(b) If $c_2 < 0$ and $a_0 - c_0 < 0$ then $\tilde{O}_1$ is also a saddle, but with the sectors in a different position as in the previous case. Going back to systems (4.2) we obtain phase portrait L_2 of Figure 2.

(c) If $c_2 > 0$ and $a_0 - c_0 < 0$ then $\tilde{O}_1$ is a stable topological node as represented in Figure 4(a). If we multiply by v to go back to systems (4.2), then all the points of the u-axis become singular points and the orientation of the orbits in the third and fourth quadrants is reversed. We obtain the local phase portrait in Figure 4(b), which is L_3 of Figure 2.

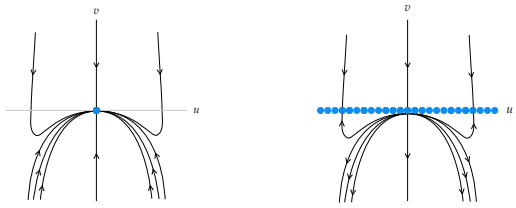

(a) Origin of systems (4.3) (b) Origin of systems (4.2)

Figure 4: Local phase portraits of $\tilde{O}_1$ and O_1 with $c_2 > 0$ and $a_0 - c_0 < 0$.

(d) If $c_2 < 0$ and $a_0 - c_0 > 0$ then $\tilde{O}_1$ is also a stable topological node, but with the sectors in a different position as in the previous case. Going back to systems (4.2) we obtain phase portrait L_4 of Figure 2.

4.2. Case with $\tilde{O}_1$ linearly zero

In this subsection we study the local phase portrait of the origin of systems (4.3) assuming $c_1 = 0$. In order to do that we use the blow up technique. First we note that the characteristic polynomial is $\mathcal{F} = -c_2u^3 - c_3u^2v - c_0uv^2$, which can not be identically zero because $c_2 \neq 0$, so the singular point $\tilde{O}_1$ is nondicritical.

Now we introduce the variable w_1 by means of the variable change $uw_1 = v$, and we obtain the systems:

$$\dot{u} = (c_0 - a_0)u^2w_1, \quad \dot{w_1} = -c_0uw_1^2 - c_3uw_1 - c_2u. \tag{4.5}$$

We eliminate a common factor u so we get

$$\dot{u} = (c_0 - a_0)uw_1, \quad \dot{w_1} = -c_0w_1^2 - c_3w_1 - c_2. \tag{4.6}$$

We must study the singular points of these systems over the line $u = 0$, which are the points with the first coordinate zero and the second one a solution of the equation $-c_0w_1^2 - c_3w_1 - c_2 = 0$. In the following we will distinguish several subcases.

(A) If $c_0 = 0$ and $c_3 = 0$, then there are no singular points over the line $u = 0$, as $c_2 \neq 0$ by hypothesis.

Subcase (A.1). If $c_2 > 0$ we have for systems (4.6) the phase portrait given in Figure 5(a). If we multiply by u, then all the points over the w_1-axis become singular points, and the orbits on the second and third

quadrants reverse their orientation, so we get phase portrait in Figure 5(b). If we undo the blow up, contracting the exceptional divisor to the origin, and swapping the second and third quadrants, we obtain for systems (4.3) the phase portrait on Figure 5(c). Lastly, if we multiply by v we get the local phase portrait for O_1, the origin of systems (4.2), which has a line consisting of singular points, the u-axis, and it is the phase portrait L_5 given in Figure 2.

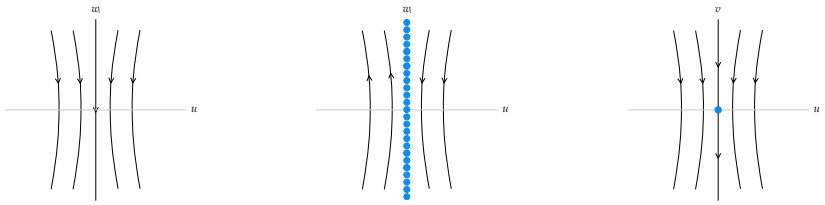

(a) (b) (c)

Figure 5: Desingularization of the origin of systems (4.2) with $c_0 = c_1 = c_3 = 0$ and $c_2 > 0$.

Subcase (A.2). If $c_2 < 0$ the vertical blow up does not determine the phase portrait, it only give us the information that over the u-axis the flow is vertical and it goes in the positive sense. We must do a horizontal blow up to determine the phase portrait. In systems (4.3) we introduce the variable w_2 by means of the change $vw_2 = u$, and with the hypothesis of this case we get the systems

$$\dot{w_2} = c_2 w_2^3 v, \quad \dot{v} = -c_2 w_2^2 v - a_0 v^2. \tag{4.7}$$

Eliminating a common factor v we obtain

$$\dot{w_2} = c_2 w_2^3, \quad \dot{v} = -c_2 w_2^2 - a_0 v, \tag{4.8}$$

and for these systems the only singular point over the line $v = 0$ is the origin, which is semi-hyperbolic. Applying Theorem 2.19 in [14] we obtain that it is a stable topological node. The phase portrait around the origin for systems (4.8) is the one in Figure 6(a), and multiplying by v, the phase portrait for systems (4.7) is the one in Figure 6(b). Undoing the blow up, contracting the exceptional divisor into the origin and swapping the third and fourth quadrants, we get that in the first and second quadrants the orbits arrive to the origin tangent to the v-axis and in the third and fourth qudrants the orbits leave the origin tangent to the v-axis, this together with the information from the vertical blow up leads to the phase portrait in Figure 6(c). At last, if we multiply again by v we obtain the local phase portrait for O_1 which is L_6 of Figure 2.

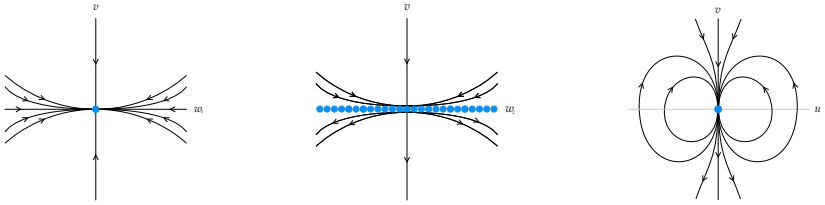

(a) (b) (c)

Figure 6: Desingularization of the origin of systems (4.2) with $c_0 = c_1 = c_3 = 0$ and $c_2 < 0$.

(B) If $c_0 = 0$ and $c_3 > 0$ then we have the hyperbolic singular point $Q_1 = (0, -c_2/c_3)$. At this point the eigenvalues of the Jacobian matrix are $a_0 c_2/c_3$ and $-c_3$ so we have two subcases.

Subcase (B.1). If $c_2 > 0$ the vertical blow up does not determine the behaviour of the orbits around the v-axis in the second and fourth quadrants. Then we do a horizontal blow up introducing the variable

$vw_2 = u$ in systems (4.3):

$$\dot{w_2} = c_2 w_2^3 v + c_3 w_2^2 v, \quad \dot{v} = -c_2 w_2^2 v + c_3 w_2 v^2 - a_0 v^2, \tag{4.9}$$

and we eliminate a common factor v:

$$\dot{w_2} = c_2 w_2^3 - c_3 w_2^2, \quad \dot{v} = -c_2 w_2^2 v - c_3 w_2 v - a_0 v. \tag{4.10}$$

For systems (4.10) there are two singular points over the line $v = 0$, the origin which is a semi-hyperbolic saddle-node and the point $(-c_3/c_2, 0)$ which is a saddle. The phase portrait around the w_2-axis for systems (4.10) is the one in Figure 7(a), and multiplying by v, the phase portrait for systems (4.9) is the one in Figure 7(b). Undoing the blow up we get the phase portrait in Figure 7(c). Finally, if we multiply again by v we obtain the local phase portrait for O_1 which is L_7 of Figure 2.

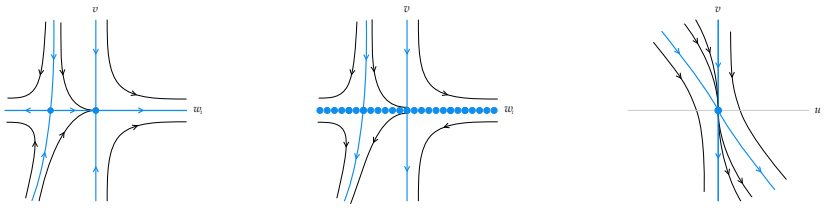

(a) (b) (c)

Figure 7: Desingularization of the origin of systems (4.2) with $c_0 = c_1 = 0$, $c_3 > 0$ and $c_2 < 0$.

Subcase (B.2). If $c_2 < 0$ then Q_1 is a stable node. We must do again a horizontal blow up to determine the local phase portrait, and thus we obtain again the phase portrait L_6 of Figure 2.

(C) If $c_0 \neq 0$, $c_3 = 0$ and $c_0 c_2 > 0$, there are no singular points over $u = 0$.

Subcase (C.1). If c_0 and c_2 are positive, we obtain again the phase portrait L_5 of Figure 2 by undoing the blow up.

Subcase (C.2). If c_0 and c_2 are negative, we obtain again the phase portrait L_6 of Figure 2, but in this case it is necessary to do a horizontal blow up to conclude.

(D) If $c_0 \neq 0$, $c_3 = 0$ and $c_0 c_2 < 0$, there are two hyperbolic singular points over $u = 0$, namely, $Q_2 = (0, \sqrt{-c_2/c_0})$ and $Q_3 = (0, -\sqrt{-c_2/c_0})$. By studying the eigenvalues of the Jacobian matrix at both points, we distinguish three subcases.

Subcase (D.1). If $c_0 > 0$ and $a_0 - c_0 > 0$ then Q_2 is a stable node and Q_3 is an unstable node. Undoing the blow up we obtain phase portrait L_6 of Figure 2.

Subcase (D.2). If $c_0 > 0$ and $a_0 - c_0 < 0$ then Q_2 and Q_3 are saddle points with the orientation of the hyperbolic orbits given in Figure 8(a). If we multiply by u and then we undo the blow up we obtain, respectively, the phase portraits in Figure 8(b) and (c). Multiplying by u again we obtain that the local phase portrait for O_1 is L_8 of Figure 2.

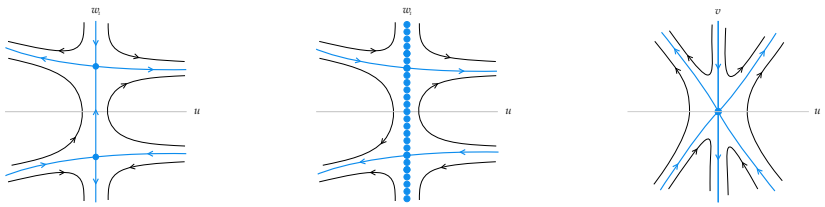

(a) (b) (c)

Figure 8: Desingularization of the origin of systems (4.2) with $c_3 = 0$, $c_0 > 0$, $c_2 < 0$ and $a_0 - c_0 < 0$.

Subcase (D.3). If $c_0 < 0$ and $a_0 - c_0 > 0$ then Q_2 and Q_3 are saddle points with a different orientation than in the previous case. Now the vertical blow up does not determine the behaviour of the orbits around the v-axis, so we must do a horizontal blow up introducing the variable w_2 such that $vw_2 = u$:

$$\dot{w}_2 = c_2 w_2^3 v + c_0 w_2 v, \quad \dot{v} = -c_2 w_2^2 v - a_0 v^2, \tag{4.11}$$

and we eliminate a common factor v:

$$\dot{w}_2 = c_2 w_2^3 + c_0 w_2, \quad \dot{v} = -c_2 w_2^2 - a_0 v. \tag{4.12}$$

For systems (4.12) there are three singular points over the line $v = 0$, the origin which is a stable node, and two saddle points $(\pm\sqrt{-c_0/c_2}, 0)$. The phase portrait around the w_2-axis for systems (4.12) is the one in Figure 9(a). If we multiply by v we get the phase portrait in Figure 9(b) for systems (4.11). Blowing down we obtain the phase portrait in Figure 9(c). If we multiply again by v we obtain the local phase portrait for O_1 which is L_9 of Figure 2.

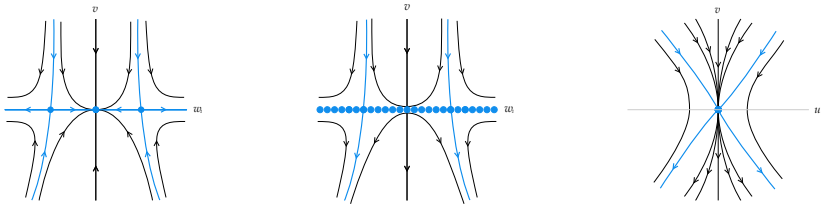

(a) (b) (c)

Figure 9: Desingularization of the origin of systems (4.2) with $c_3 = 0$, $c_0 < 0$, $c_2 > 0$ and $a_0 - c_0 > 0$.

(E) If $c_0 \neq 0$, $c_3 \neq 0$ and $c_3^2 - 4c_0c_2 < 0$ then there are no singular points over $u = 0$.

Subcase (E.1). If $c_2 > 0$ we obtain phase portrait L_5 of Figure 2.

Subcase (E.2). If $c_2 > 0$ it is necessary to do a horizontal blow up and thus we obtain the phase portrait L_6 of Figure 2.

(F) If $c_0 \neq 0$, $c_3 \neq 0$ and $c_3^2 - 4c_0c_2 > 0$ then there are two hyperbolic singular points over $u = 0$, namely, $Q_4 = (0, -(c_3 + \sqrt{c_3^2 - 4c_0c_2})/(2c_0))$ and $Q_5 = (0, -(c_3 - \sqrt{c_3^2 - 4c_0c_2})/(2c_0))$.

Subcase (F.1). If $a_0 - c_0 > 0$, $c_0 > 0$ and $R_c - c_3 > 0$ then Q_4 is an unstable node and Q_5 a stable node. Blowing down we obtain phase portrait L_6 of Figure 2.

Subcase (F.2). If $a_0 - c_0 > 0$, $c_0 > 0$ and $R_c - c_3 < 0$ then Q_4 is an unstable node and Q_5 a saddle. Blowing down we obtain phase portrait L_7 of Figure 2.

Subcase (F.3). If $a_0 - c_0 > 0$, $c_0 < 0$ and $R_c - c_3 > 0$ then Q_4 and Q_5 are saddle points, but the vertical blow up does not determine the behaviour of the orbits around the v-axis. Doing a horizontal blow up we obtain phase portrait L_9 of Figure 2.

Subcase (F.4). If $a_0 - c_0 > 0$, $c_0 < 0$ and $R_c - c_3 < 0$ then Q_4 is a saddle and Q_5 is a stable node. Again the vertical blow up is not enough to determine the phase portrait. With a horizontal blow up we obtain phase portrait L_{10} of Figure 2.

Subcase (F.5). If $a_0 - c_0 < 0$, $c_0 > 0$ and $R_c - c_3 > 0$ then Q_4 and Q_5 are saddle points. Blowing down we obtain phase portrait L_8 of Figure 2.

Subcase (F.6). If $a_0 - c_0 < 0$, $c_0 > 0$ and $R_c - c_3 < 0$ then Q_4 is a saddle and Q_5 is a stable node. Blowing down we obtain phase portrait L_{11} of Figure 2.

(G) If $c_0 \neq 0$, $c_3 \neq 0$ and $c_3^2 - 4c_0c_2 = 0$ then we have the singular point $Q_6 = (0, -c_3/(2c_0))$, which is a semi-hyperbolic saddle-node. Attending to the position of the different sectors we have the following cases.

Subcase (G.1). If $c_0(a_0 - c_0) > 0$ and $c_0 > 0$, blowing down we obtain phase portrait L_7 of Figure 2.

Subcase (G.2). If $c_0(a_0 - c_0) < 0$ and $c_0 > 0$, blowing down we obtain phase portrait L_{11} of Figure 2.

Subcase (G.3). If $c_0(a_0 - c_0) < 0$ and $c_0 < 0$ the vertical blow up does not determine the phase portrait of O_1. Doing a horizontal blow up we get the phase portrait L_{12} of Figure 2.

5. Global phase portraits

In this section we bring together the local information obtained in Sections 3 and 4 to prove Theorem 1.1. In each case of Tables 2 to 7, the conditions determine the phase portrait of O_1, i.e., only one of the local phase portraits L_1 to L_{12} in Figure 2 can appear in each case, except in case 4.2. In this case 4.2 we must distinguish two cases determined by the sign of $a_0 - c_0$.

Once determined the local phase portrait at the singular points, in most cases the place where born and die the separatrices is determined in a unique way. We draw these separatrices, one orbit in each canonical region which does not have an inifinite number of singular points in the boundary, and three orbits (representing the infinite number of them existing) in each canonical region with an infinite number of singular points in the boundary. Thus we obtain the global phase portraits in Figure 15. In Table 8 we indicate which is the global phase portrait obtained in each case from the ones included in Figure 15.

Now we focus on the cases in which the separatrices can be connected in three different ways, namely 1.8, 1.9, 2.4, 2.5, 3.2 and 3.3. In the following we explain how it can be determined which of the three options is realizable.

Case 1.8. By Theorem 4.8(1) in [11] we know that on any straight line $z = cte \neq 0$ there exists exactly one contact point. Two of the three global phase portraits obtained by connecting the separatrices contradict this result. In both cases, if we take the line $z = (R_c - c_3)/2c_2$ we can find two contact points on it, one is the singular point P_1 and the other is a point on the third quadrant, as shown in Figure 10. We can ensure the existence of this contact point as if we choose, for example, the point indicated with a square in Figure 10, the orbit passing through this point has as α-limit the origin and as ω-limit the singular point P_4, i. e. it is an orbit as the one drawn with dashed line, and that allow to prove the existence of the contact point indicated with a cross. The same occurs in the two phase portraits included in Figure 10, then we can conclude that these two phase portraits are no realizable, and there is only one global phase portrait in case 1.8, and it is the G8 as it is indicated in Table 8.

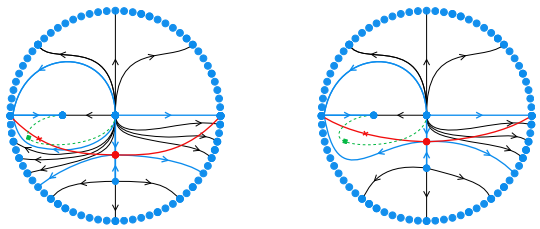

Figure 10: Global phase portraits appearing on case 1.8 that are not realizable.

Case 1.9. Here we can apply the same result than in the previous case to dismiss two global phase portraits. If we take a straight line $z = z_0$ with $-(R_c + c_3)/(2c_2) < z_0 < (R_c - c_3)/(2c_2)$, then over this line there are two contact points, one in the third quadrant and other in the fourth quadrant, as shown in Figure 11. Thus the only global phase portrait in case 1.9 is the G9.

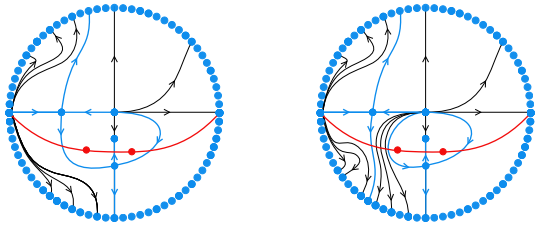

Figure 11: Global phase portraits appearing on case 1.9 that are not realizable.

Case 2.4. In this case we obtain first three possible global phase portraits by applying Corollary 4.3 in [11], because it ensures that the phase portraits must be symmetric with respect to the z-axis. Otherwise we would have more possible phase portraits. Then, by Theorem 4.8(2) in [11], we know that there must exist two invariant straight lines $z = (-c_3 \pm R_c)/(2c_2)$, i.e., the lines $z = cte$ passing through the singular points P_1 and P_2. This is only possible in one of the three global phase portraits obtained by connecting the separatrices, namely in the G14 of Figure 15. In the other two global phase portraits these two invariant lines does not exist, as can be seen in Figure 12.

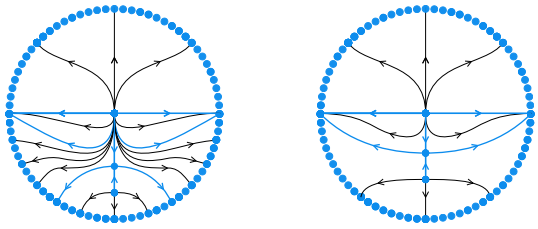

Figure 12: Global phase portraits appearing on case 2.4 that are not realizable.

Case 2.5. Here we can use the same arguments than in the previous case to prove that the only realizable phase portrait is the G15, so we will not give more details.

Case 3.2. We must apply again Theorem 4.8(1) in [11]. In two of the three global phase portraits obtained connecting the separatrices, if we take the line $z = -c_3/(2c_2)$ we can find two contact points on it, one is the singular point P_3 and the other is a point on the third quadrant, as shown in Figure 13. Thus, this two phase portraits are no realizable, and the only global phase portrait in case 3.2 is the G20, as indicated in Table 8.

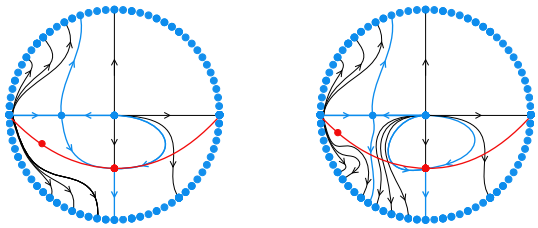

Figure 13: Global phase portraits appearing on case 3.2 that are not realizable.

Case 3.3. The same arguments that in the previous case are valid here. In Figure 14 the line with two contact points is represented in the two global phase portraits that are indeed not realizable. The only possible phase portrait in this case is the G21 of Figure 15.

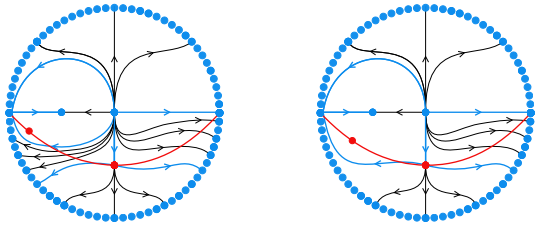

Figure 14: Global phase portraits appearing on case 3.3 that are not realizable.

Case	**Subcase**	O_1	**Global**
1.1		L_4	G1
1.2		L_1	G2
1.3		L_3	G3
1.4		L_2	G4
1.5		L_4	G5
1.6		L_1	G6
1.7		L_4	G7
1.8		L_1	G8
1.9		L_3	G9
1.10		L_2	G10
2.1		L_{10}	G11
2.2		L_9	G12
2.3		L_6	G13
2.4		L_7	G14
2.5		L_{11}	G15
2.6		L_8	G16
2.7		L_6	G17
2.8		L_7	G18
3.1		L_4	G19
3.2		L_3	G20
3.3		L_1	G21
3.4		L_3	G22
3.5		L_4	G23
3.6		L_1	G24
4.1		L_{12}	G25
4.2	$a_0 - c_0 > 0$	L_7	G26
	$a_0 - c_0 < 0$	L_{11}	G27
4.3		L_6	G28
4.4		L_5	G29
5.1		L_3	G30
5.2		L_4	G23
5.3		L_3	G31
5.4		L_1	G24
6.1		L_6	G28
6.2		L_5	G29

Table 8: Classification of global phase portraits of systems 1.3

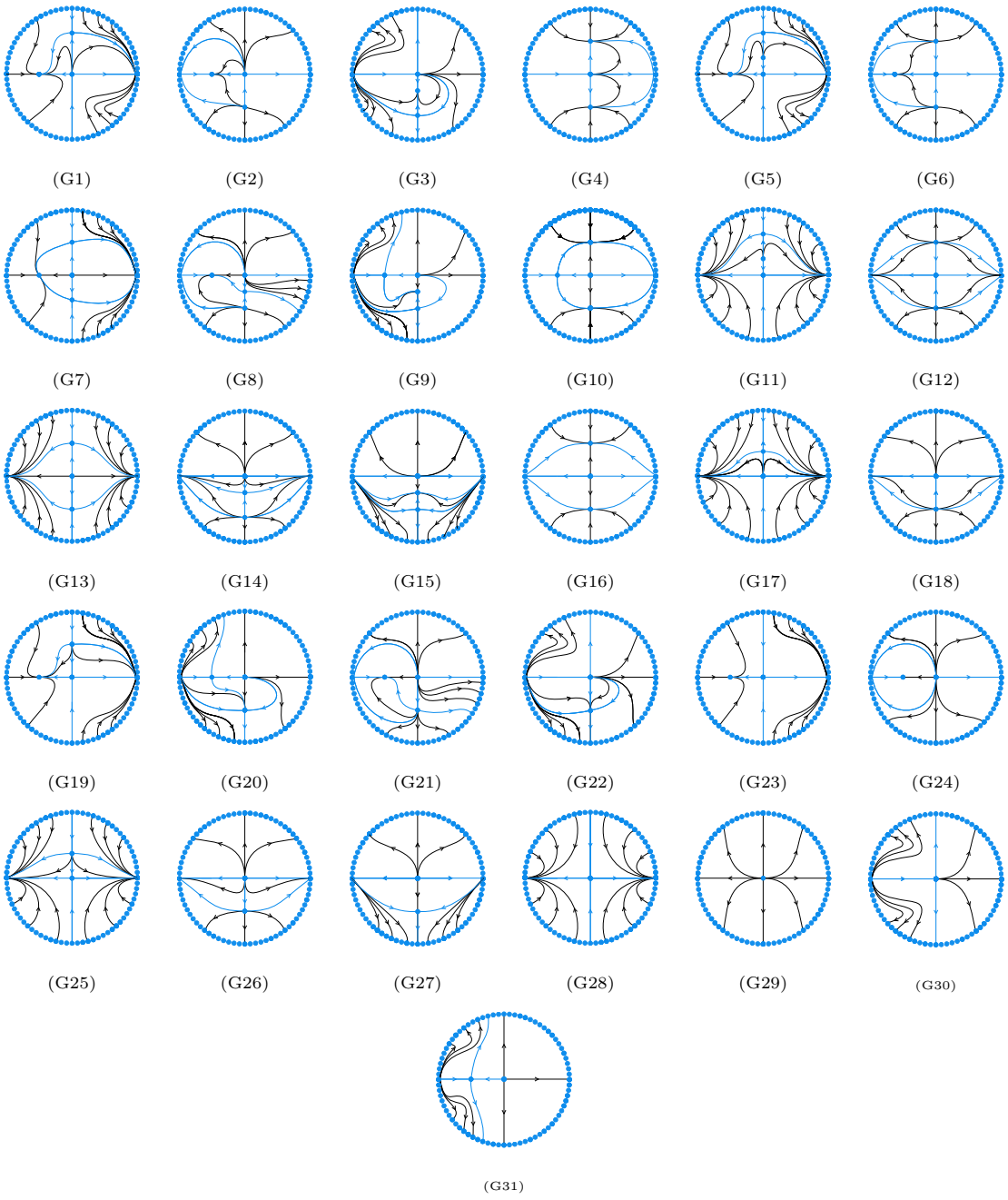

Figure 15: Global phase portraits of systems (1.3) in the Poincaré disc.

We have obtained 34 global phase portraits given in Figure 15, but some of them are topologically equivalent so we must study these equivalences. Note that in order to apply Theorem 2.1 and determine which of them are topologically equivalent by studying the separatrix skeleton we consider only the open Poincaré disc. We will distinguish classes of equivalence according to the following invariants: the number of finite singular points and the sum of the indices at the finite singular points, denoted by ind_F. This classification is given in Table 9. Then within each class we prove which of the phase portraits are topologically equivalent.

Class	Nº finite singular points	ind_F	Global phase portraits
1	4	0	G5,G7,G9.
2		2	G6,G8,G10.
3	3	-1	G11,G13.
4		0	G1, G3, G19, G20.
5		1	G12,G14,G15.
6		2	G2,G4,G21.
7		3	G16.
8	2	-1	G17, G25.
9		0	G22, G23, G31.
10		1	G18, G26, G27.
11		2	G24.
12	1	-1	G28.
13		0	G30.
14		1	G29.

Table 9: Classes of equivalence according to the number of finite singular points and to the ind_F.

Class 1. Global phase portrait G5 is topologically equivalent to G7 because if we move the unstable node in G5 to the origin we obtain G7. G5 is topologically distinct to G9 as in G9 all the orbits arriving to the stable node come from the unstable node or from a unique infinite singular point while in G5 there are orbits that arrive to the stable node from infinitely many infinite singular points. Then in this class there are two topologically different phase portraits represented by G5 and G9.

Class 2. G6 is topologically equivalent to G10 by moving the stable node in G6 to the origin, doing a symmetry with respect to the z-axis and doing a change of the time variable t by $-t$. G6 is different from G8 because in G6 there are four separatrices that connect inifinite singular points with finite singular points and in G8 there are five separatrices of this kind. In this class there are two topologically different phase portraits represented by G6 and G8.

Class 3. G11 is topologically equivalent to G12 by moving the node in G11 to the origin. Then in this class there is only one topologically different phase portrait.

Class 4. G1 is different from G3 as to the node in G1 arrive orbits from ininitely many infinite singular points but in G3 only from one infinite singular point. G1 is topologically equivalent to G19 by moving the saddle in G1 to the origin and doing a symmetry with respect to the x-axis. G1 is topologically equivalent to G20: we must move the saddle in G20 to the origin and the unstable node to the positive x-axis, and then the saddle-node to the origin and the saddle to the positive z-axis. Then we must do a symmetry with respect to the z- axis and a change of the time variable t by $-t$. In this class there are two topologically different phase portraits represented by G1 and G3.

Class 5. G12 is topologically equivalent to G14 by moving the saddle in G14 to the origin. G14 is different from G15 because in both global phase portraits there are two nodes, but in G14 they have the same stability and in G15 one is stable and the other is unstable. In this class there are two topologically different phase portraits represented by G12 and G15.

Class 6. G2 is different from G4 because in both phase portraits there are two nodes, but in G2 they have different stability and in G4 the same. G21 is different from G2 and G4 because in G2 and G4 there are 9 separatrices in the open Poincaré disc and in G21 there are 10 separatrices. Then in this class all the phase portraits are topologically different.

Class 8. G17 is topologically equivalent to G25 by moving the saddle-node in G17 to the origin and doing a symmetry with respect to the x-axis. Then in this class there is only one topologically different phase portrait.

Class 9. G22 is different from G23 because they have different kind of finite singular points. G23 is topologically equivalent to G31 by moving the node in G23 to the origin, doing a symmetry with respect to the z-axis and a change of the time variable t by $-t$. In this class there are two topologically different phase portraits represented by G22 and G23.

Class 10. G18 is topologically equivalent to G26 by moving the node in G18 to the origin and doing a symmetry with respect to the x-axis. G26 is different from G27 because in G26 there are a separatrix that connects two finite singular points and in G27 there is not a such separatrix. In this class there are two topologically different phase portraits represented by G18 and G27.

Note that classes 7,11,12,13 and 14 have only one global phase portrait each of them. In summary, we have obtained 22 different phase portraits in the Poincaré disc for systems (1.3), so we have proved Theorem 1.1. This 22 phase portraits are described in Figure 1, where we include a representative of each one of the topological equivalence classes. These representatives correspond with the phase portraits in Figure 15 as follows:

Rep.	Phase portraits
R1	G1, G19, G20.
R2	G2.
R3	G3.
R4	G4.
R5	G5, G7.
R6	G6, G10.
R7	G8.
R8	G9.

Rep.	Phase portraits
R9	G11, G13.
R10	G12, G14.
R11	G15.
R12	G16.
R13	G17, G25.
R14	G18, G26.
R15	G21.
R16	G22.

Rep.	Phase portraits
R17	G23, G31.
R18	G24.
R19	G27.
R20	G28.
R21	G29.
R22	G30.

Acknowledgements

The first and third authors are partially supported by the Ministerio de Economía, Industria y Competitividad, Agencia Estatal de Investigación (Spain), grant MTM2016-79661-P (European FEDER support included, UE) and the Consellería de Educación, Universidade e Formación Profesional (Xunta de Galicia), grant ED431C 2019/10 with FEDER funds. The first author is also supported by the Ministerio de Educacion, Cultura y Deporte de España, contract FPU17/02125.

The second author is partially supported by the Ministerio de Ciencia, Innovación y Universidades, Agencia Estatal de Investigación grant PID2019-104658GB-I00, the Agència de Gestió d'Ajuts Universitaris i de Recerca grant 2017SGR1617, and the H2020 European Research Council grant MSCA-RISE-2017-777911.

Bibliography

[1] J. Alavez-Ramírez, G. Blé, V. Castellanos and J. Llibre, *On the global flow of a 3-dimensional Lotka-Volterra system*, Nonlinear Anal.-Theory Methods Appl., **75** (2012), 4114-4125.

[2] M. J. Álvarez, A. Ferragut and X. Jarque, *A survey on the blow up technique*,Int. J. Bifurcation Chaos, **21**(11) (2011) 3103–3118.

[3] A. A. Andronov, E. A. Leontovich, I.J. Gordon and A. G. Maier, *Qualitative Theory of 2nd Order Dynamic Systems*, J. Wiley & Sons, (1973).

[4] A. Arneodo, P. Coullet, P., C. Tresser, *Occurrence of strange attractors in three-dimensional Volterra equations*, Phys. Lett., **79A**, 259–263.

[5] G. Blé, V. Castellanos, J. Llibre, I. Quintalán, *Integrability and global dynamics of the May-Leonard model*, Nonlinear Anal.-Real World Appl., **14** (2013), 280–293.

[6] C. A. Buzzi, R. A. T. Santos, J. Llibre, *Final evolutions of a class of May-Leonard Lotka-Volterra systems*, J. Nonlinear Math. Phys., **27**(2) (2020), 267–278.

[7] P. Breitenlohner, G. Lavrelashvili and D. Maison, *Mass inflamation and chaotic behaviour inside hairy black holes*, Nucl. Phys. B, **524** (1998), 427–443.

[8] F.H. Busse, *Transition to turbulence via the statistical limit cycle route*, Synergetics, **39**, (1978), Springer-Verlag, Berlin.

[9] J. Coste, J. Peyraud, P. Coullet, *Asymptotic Behaviors in the Dynamics of Competing Species*, SIAM J. Appl. Math. **36**(3), 516–543.

[10] R. L. Devaney, *Collision Orbits in the Anisotropic Kepler Problem*, Invent. Math. (1978), **45**, 221-251.

[11] E. Diz-Pita, J. Llibre and M. V. Otero-Espinar, *Phase portraits of a family of Kolmogorov systems depending on six parameters*, Electron. J. Differ. Equ., **35** (2021), 1–38.

[12] E. Diz-Pita, J. Llibre and M. V. Otero-Espinar, *Planar Kolmogorov systems coming from spatial Lotka-Volterra systems*, To appear on International Journal of Bifurcation and Chaos.

[13] F. Dumortier, *Singularities of vector fields on the plane*, J. Diff. Eq., **23** (1977) 53–106.

[14] F. Dumortier, J. Llibre and J.C. Artés, *Qualitative Theory of Planar Differential Systems*, UniversiText, Springer-Verlag, New York, 2006.

[15] X. Fu, P. Zhang, J. Zhang, *Forecasting and Analyzing Internet Users of China with Lotka-Volterra Model*, Asia-Pac J. Oper. Res., **34** (2017), 1749996.

[16] G. Gandolfo, *Economic dynamics*, Fourth edition. Springer, Heidelberg, 2009.

[17] G. Gandolfo, *Giuseppe Palomba and the Lotka-Volterra equations*, Rend. Lincei-Mat. Appl., **19**(4) (2008), 347–357.

[18] R. Hering, *Oscillations in Lotka-Volterra systems of chemical reactions*, J. Math. Chem. **5** (1990), 197–202.

[19] M. Hirsch, C. Pugh, M. Shub, *Invariant Manifolds*, Lecture Notes in Mathematics, Vol. 583. Springer-Verlag, 1977.

[20] G. Laval and R. Pellat, *Plasma Physics*, Proceedings of Summer School of Theoretical Physics, Gordon and Breach, NY, 1975.

[21] P. Leach, J. Miritzis, *Competing species: Integrability and stability*, J. Nonlinear Math. Phys., **11** (2006), 123–133.

[22] J. Llibre, Y. Martínez, *Dynamics of a competitive Lotka-Volterra system in* $\mathbb{R}^3$, Acta Appl. Math. **170**, 569–577.

[23] J. Llibre, Y. P. Martínez, *Dynamics of a family of Lotka-Volterra systems in* $\mathbb{R}^3$, Nonlinear Analysis, **199** (2020), 111915.

[24] J. Llibre, Y. Martínez, *Global dynamics of a Lotka-Volterra system in* $\mathbb{R}^3$, J. Nonlinear Math. Phys., **27**(3) (2020), 509–519.

[25] J. Llibre, C. Valls, *Polynomial, rational and analytic first integrals for a family of 3-dimensional Lotka-Volterra systems*, Zeitschrift fur angewandte Mathematik und Physik, **62**(5) (2011), 761–777.

[26] J. Llibre, D. M. Xiao, *Global dynamics of a Lotka-Volterra model with two predators competing for one prey*, SIAM K. Appl. Math. **74**(2), 434–453.

[27] C. Lois-Prados, R. Precup, *Positive periodic solutions for Lotka-Volterra systems with a general attack rate*, Nonlinear Anal.-Real World Appl., **52** (2020), 103024.

[28] L.Markus, *Global structure of ordinary differential equations in the plane*, Trans. Amer. Math. Soc., **76** (1954), 127–148.

[29] D.A. Neumann, *Classification of continuous flows on 2-manifolds*, Proc. Amer. Math. Soc., **48** (1975), 73–81.

[30] M. M. Peixoto, *Proccedings of a simposium held at the university of Bahia*, Acad. Press, New York (1973), 349–420.

[31] D. Schlomiuk and N. Vulpe, *Global topological classification of Lotka-Volterra quadratic differential systems*, Electron. J. Differ. Equ., **64** (2012), 1–69.

[32] S. Smale, *On the differential equations of species in competition*, J. Math. Biology, **3** (1976), 5–7.

[33] R. M. Tudoran, A. Girban, *On a hamiltonian version of a three-dimensional Lotka-Volterra system*, Nonlinear Anal.-Real World Appl., **13** (2012), 2304–2312.

[34] A. W. Wijeratne, F. Yi and J. Wei, *Bifurcation analysis in the diffusive Lotka-Volterra system: an application to market economy*, Chaos Solitons Fractals, **40**(2), (2009), 902-911.